

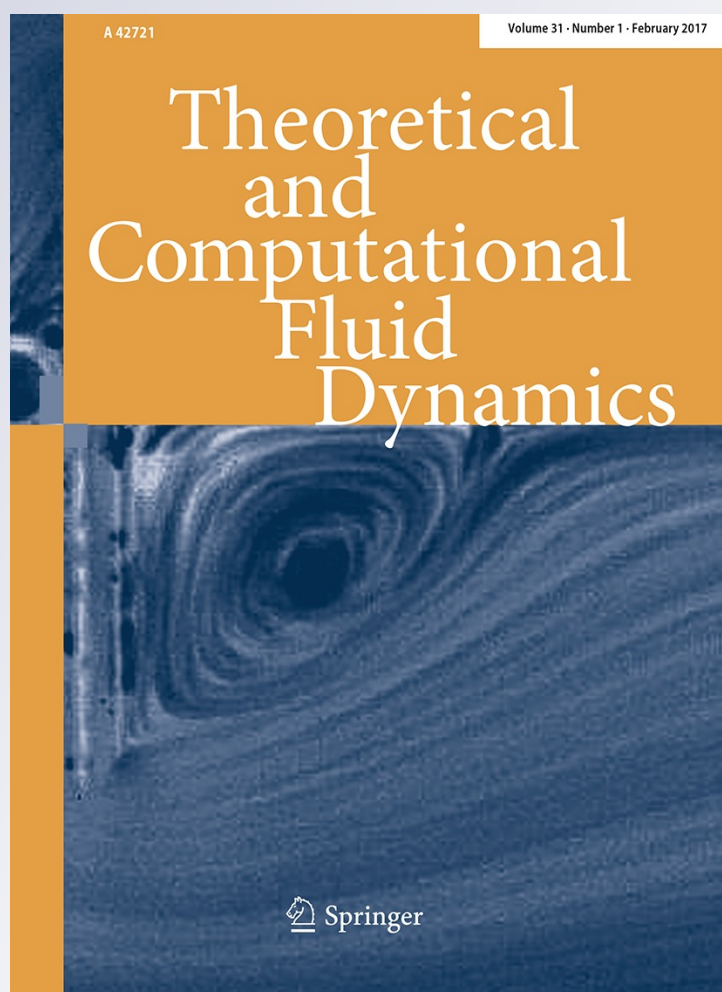
Excitation of unsteady Görtler vortices by localized surface nonuniformities

**A. V. Boiko, A. V. Ivanov,
Yu. S. Kachanov, D. A. Mischenko &
Yu. M. Nechepurenko**

**Theoretical and Computational Fluid
Dynamics**

ISSN 0935-4964
Volume 31
Number 1

Theor. Comput. Fluid Dyn. (2017)
31:67-88
DOI 10.1007/s00162-016-0404-y



Your article is protected by copyright and all rights are held exclusively by Springer-Verlag Berlin Heidelberg. This e-offprint is for personal use only and shall not be self-archived in electronic repositories. If you wish to self-archive your article, please use the accepted manuscript version for posting on your own website. You may further deposit the accepted manuscript version in any repository, provided it is only made publicly available 12 months after official publication or later and provided acknowledgement is given to the original source of publication and a link is inserted to the published article on Springer's website. The link must be accompanied by the following text: "The final publication is available at link.springer.com".



ORIGINAL ARTICLE

A. V. Boiko  · A. V. Ivanov · Yu. S. Kachanov ·
D. A. Mischenko · Yu. M. Nechepurenko

Excitation of unsteady Görtler vortices by localized surface nonuniformities

Received: 28 April 2015 / Accepted: 5 August 2016 / Published online: 25 August 2016
© Springer-Verlag Berlin Heidelberg 2016

Abstract A combined theoretical and numerical analysis of an experiment devoted to the excitation of Görtler vortices by localized stationary or vibrating surface nonuniformities in a boundary layer over a concave surface is performed. A numerical model of generation of small-amplitude disturbances and their downstream propagation based on parabolic equations is developed. In the framework of this model, the optimal and the modal parts of excited disturbance are defined as solutions of initial-value problems with initial values being, respectively, the optimal disturbance and the leading local mode at the location of the source. It is shown that a representation of excited disturbance as a sum of the optimal part and a remainder makes it possible to describe its generation and downstream propagation, as well as to predict satisfactorily the corresponding receptivity coefficient. In contrast, the representation based on the modal part provides only coarse information about excitation and propagation of disturbance in the range of parameters under investigation. However, it is found that the receptivity coefficients estimated using the modal parts can be reinterpreted to preserve their practical significance. A corresponding procedure was developed. The theoretical and experimental receptivity coefficients are estimated and compared. It is found that the receptivity magnitudes grow significantly with the disturbance frequency. Variation of the span-wise scale of the nonuniformities affects weakly the receptivity characteristics at zero frequency. However, at high frequencies, the efficiency of excitation of Görtler vortices depends substantially on the span-wise scale.

Keywords Boundary layer · Görtler vortices · Surface roughness · Surface vibrations · Receptivity · Instability · Optimal disturbances · Local modes

1 Introduction

The Görtler instability may emerge in boundary layers over concave surfaces under the action of centrifugal forces in a wide range of free-stream speeds and Mach numbers [48]. Such instability is able to lead to formation of stream-wise vortices, which may exhibit a distinct growth in the stream-wise direction altering significantly heat and mass transfers, affecting skin friction, leading to flow turbulization and modifying other

Communicated by Dr. M.R. Malik.

A. V. Boiko (✉) · A. V. Ivanov · Yu. S. Kachanov · D. A. Mischenko
Khristianovich Institute of Theoretical and Applied Mechanics, Novosibirsk, Russia 630090
E-mail: boiko@itam.nsc.ru

A. V. Boiko
Tyumen State Oil and Gas University, Tyumen, Russia 625000

Yu. M. Nechepurenko
Institute of Numerical Mathematics, Moscow, Russia 119333

flow parameters important for various applications. Therefore, problems of excitation and evolution of steady and unsteady Görtler vortices are of great importance for aerodynamic devices and vehicles, as well as for their components with curved aerodynamic surfaces such as air inlets of engines, blades of turbo-machines, flaps and slats. Hence, the problem of Görtler instability has been investigated for a long time experimentally, theoretically and numerically (see, e.g., reviews in [9, 19, 20, 30, 48]). The majority of these studies are devoted to *stationary* Görtler vortices.

For the first time, the stream-wise vortices, associated with the centrifugal instability of the shear flow between two rotating cylinders, were found and studied both theoretically and experimentally by Taylor [59]. Experiments by Clauser and Clauser [14] showed that the laminar boundary layers over concave walls become turbulent at lower Reynolds numbers than those over flat or convex surfaces that indicated the presence of a similar instability mechanism. Later Görtler [24], using the approximation of a locally parallel undisturbed flow, developed a normal-mode approach to show that the same kind of instability can occur in boundary layers over concave surfaces when a certain parameter $G\ddot{o} = Re\sqrt{\delta}/R$, called the Görtler number, exceeds a critical value. Here Reynolds number is defined as $Re = U_e\delta/\nu$, where the length δ characterizes the boundary-layer thickness, U_e is the free-stream velocity at the boundary-layer edge, ν denotes the kinematic viscosity of the fluid, and R is the radius of wall curvature. The critical Görtler number depends on the disturbance span-wise wave-number β (normalized usually by the length scale δ). The dependence $G\ddot{o}(\beta)$ forms a neutral stability curve defined, for stationary instability modes, in the $(G\ddot{o}, \beta)$ -plane. For traveling (nonstationary) Görtler vortices, there is a family of neutral curves in the $(G\ddot{o}, \beta)$ -plane for various fixed values of the disturbance frequency ω or, alternatively, there is a neutral stability surface in the three-dimensional $(G\ddot{o}, \beta, \omega)$ -space.

A direct connection between the earlier boundary-layer turbulization on concave surfaces found in [14] and Görtler instability has been demonstrated by Liepmann [43]. First direct experimental evidences of existence of stationary Görtler vortices were obtained by the china-clay surface visualization in [25] and by the hot-wire technique in [57]. The experiments and subsequent analyses have shown that in boundary-layer flows, this instability develops in space, i.e., it has a convective character. Later, numerous flow visualizations and hot-wire measurements (see, e.g., [35]) have helped to improve significantly the understanding of this instability and to evaluate its influence on the laminar-turbulent transition in boundary layers.

A series of studies were carried out with excitation of controlled perturbations. In such experiments [6] performed in water, some span-wise periodic steady disturbances were introduced into a boundary layer by means of an array of heated stream-wise-oriented wires. The instability was detected via an observation of deformation of span-wise timelines formed by hydrogen bubbles. Some points belonging to a short-wave part of the neutral stability curve were obtained. However, the amplitudes of the excited disturbances were quite large because it would be otherwise difficult to detect them by means of the visualization method. In experiments of [1, 62], a set of thin plates located in free-stream generated steady Görtler vortices; some results obtained in [6] were reproduced, and also additional points of the neutral stability curve were documented.

However, the disturbance growth rates obtained experimentally did not agree for a long time with those calculated by the linear stability theory in the whole range of span-wise wave-numbers and Görtler numbers studied [18, 19]. One of the reasons for the discrepancy was associated with nonlinear effects because the amplitudes of the stream-wise velocity variations caused by the investigated vortices were quite large (often about 10% of free-stream speed, as in [6]). Another cause is related to the so-called transient growth of perturbations occurring in the disturbance-source near-field.

In the long-wavelength region, some serious difficulties exist in application of the local parallelism approximation to the linear stability theory. For instance, in [24, 32], the Görtler number of neutral point increases as the span-wise wave-number decreases below 0.1 (when it is normalized by the boundary-layer displacement thickness δ^*) and approaches 10 at wave-number about 0.01. Meanwhile, in calculations of [31, 55], the same Görtler number remains small and nearly constant (about 0.7–0.8), while in [20] it continues to decrease at least down to 0.1.

A great number of subsequent attempts to advance the approximation validity by means of accounting for the boundary-layer growth did not lead to an adequate solution of the problem. The disturbance growth rates predicted by various theories still differ significantly from each other and seriously disagree with the experimental data. Moreover, although according to the linear stability theory [20] the flow becomes unstable when Görtler number exceeds value of about unity, experimentalists were not able to observe Görtler vortices until $G\ddot{o}^* \approx 10$. Here and below, we denote Görtler number $G\ddot{o}^*$ when displacement thickness δ^* is used as δ : $G\ddot{o}^* = (U_e\delta^*/\nu)\sqrt{\delta^*}/R$. The significant difference between predicted and experimental growth rates is observed in the whole studied range of span-wise wave-numbers and Görtler numbers.

Hall [27,28] showed that the reduction in the problem under consideration to a set of homogeneous ordinary differential equations is not justified for values of $G\ddot{o}$ and β of order of unity and lower; the neglect of the downstream variation of the vortex shape (i.e., consideration of the wall-normal amplitude function as independent of x and prehistory of its development) is invalid in this case. To account for the prehistory, one has to formulate the problem as a set of partial differential equations and solve the corresponding parabolic initial-boundary-value problem. Numerical experiments show that the behavior of stationary vortices at small Görtler numbers depends significantly on initial conditions and determination of a unique neutral stability curve loses practical significance [11,29,45]. In such a case, the most accurate approach, which allows tracing the development of the vortices from the very beginning, consists of formulating and solving the receptivity problem to provide proper initial conditions. Excitation of steady and unsteady Görtler vortices by free-stream vortical disturbances has been studied theoretically and numerically in [66] and excitation of steady vortices induced by a stationary roughness in [3,16]. Experimentally, the receptivity problems on excitation of Görtler vortices had not been studied quantitatively until recently due to its complexity even for stationary surface roughness.

Furthermore, the situation in boundary layers is aggravated even at $\beta \gtrsim 1$ by the presence of the so-called near-field region adjoining a disturbance source, especially downstream of it. This phenomenon is related to the so-called *lift-up* effect [52], which allows for the stream-wise disturbance velocity to experience a transient algebraic (rather than exponential) growth even in a linearly stable flow. In the framework of the modal approach, this can be illustrated in terms of many attenuating modes of linearized Navier–Stokes equations with the same value of the span-wise wave-number and frequency (including zero frequency), but with different stream-wise wave-numbers [63]. The superposition of the nonorthogonal modes produced by a disturbance source can lead to a complicated behavior (including the transient growth) of the stream-wise velocity disturbance in an extended downstream area particularly at $\beta \sim 1$ characteristic for the most growing Görtler vortices. The wall-normal profiles of the stream-wise velocity disturbances often resemble the Görtler vortex profiles. This renders it difficult to distinguish these two kinds of disturbances in experiment.

The majority of technical problems occurred in previous experimental investigations of *stationary* Görtler vortices are associated with a poor accuracy of measurements of low-amplitude velocity perturbations on the background of large mean shear-flow velocity accompanied by large wall-normal gradients. In addition, some previous experimental difficulties can be attributed, at least partly, to a possible influence of nonlinearity and to the mechanism of nonmodal disturbance development discussed above or, in other words, to a large disturbance-source near-field. Due to these reasons, an accurate (and even satisfactory) agreement between the experimental growth rates of steady Görtler vortices and those predicted by the linear stability theory has never been achieved until recently (see below).

Experimental investigations of the linear Görtler instability problem in *nonstationary* formulation had also been absent until recently. The number of available theoretical and numerical results on time-periodic vortices is also very restricted, though the original Görtler equations [24] are time-dependent. The growth of Görtler instability modes in a form of unsteady, oscillating vortices as a primary state was considered in [27,33] for subsonic and in [56] for supersonic boundary layers. It has been shown that the unsteady (periodic in time) modes are less amplified compared to steady ones. This result was obtained in [27] with accounting for the effects of the base-flow nonparallelism but only in the limit of infinitely large span-wise wave-numbers. The case of $O(1)$ wave-numbers (being of the greatest practical importance) has not been studied.

The *initial-boundary-value* problem of the development of *nonstationary* disturbances in a boundary layer on a concave wall has been considered by Bertolotti [5]. The study was mainly devoted to the development of Tollmien–Schlichting (TS) waves; therefore, the Navier–Stokes equations were reduced and normalized quite differently compared to the initial-boundary-value problem for Görtler vortices formulated in [29]. Nevertheless, it was pointed out that the surface curvature promotes amplification of both the Görtler vortices and the oblique TS waves. Their instability regions were found to merge with each other as the surface curvature increases.

Based on flow visualizations and theoretical results, it is believed usually that steady vortices dominate in the flows in the presence of Görtler instability. This is plausible quite often, but cannot be rigorously justified for all practical cases. Unsteady vortices can be initiated by low-frequency vortical perturbations of incoming flows and seem to appear in many practical situations (see, e.g., [53,66]). Such perturbations are typical, for example, in boundary layers on curved blades of turbo-machines. Consequently, the apparent predominance of steady Görtler vortices in numerous experiments might be explained, for example, by a stronger boundary-layer receptivity to these disturbances, or by larger dimensionless amplitudes of surface roughness or free-stream nonuniformities in comparison with amplitudes of surface vibrations or free-stream velocity fluctuations, rather

than by their largest amplification rates. Such situation might be similar to the swept-wing boundary-layer instability, where less amplified stationary disturbances dominate frequently in the flow [22,50].

Recent investigations of *unsteady* Görtler instability (including the quasisteady case) described in [8,9] have changed the situation in the Görtler instability field significantly. Due to the application of a new experimental approach and an in-depth theoretical support of the study, a new level of agreement between the experimental and computed characteristics of the linear Görtler instability was obtained. The novel experimental procedure has allowed the authors to examine very accurately both stationary (in a quasistationary limit) and essentially nonstationary small-amplitude Görtler vortices. The results obtained in [8,9] provided a solid basis for further investigations, including a systematic study of excitation mechanisms of unsteady Görtler vortices by various external disturbances.

The importance of the base-flow receptivity to surface imperfections for the problem of excitation and development of Görtler vortices had been recognized for a long time [11,29,45]. However, until recently, this problem had been examined only theoretically and only for a particular case of stationary Görtler vortices generated by surface roughness [3,16].

First quantitative experimental investigation of the problem of excitation of stationary and nonstationary Görtler vortices by stream-wise localized surface nonuniformities (roughness elements and vibrations) had been performed in [36–38]. The experiments were carried out at controlled disturbance conditions with small surface nonuniformities when the receptivity coefficients, being defined in Fourier space, were independent of the particular shapes of the surface imperfections. These definitions of the receptivity coefficients are similar to those used in several previous studies devoted to the linear receptivity problems describing excitation of either oblique TS waves [2,39,40,49,65] or cross-flow (CF) instability modes developing in three-dimensional boundary layers [21,22] (for review, see also [41]).

However, the experimental results [36–38] need theoretical analysis due to several circumstances. In particular, it is not clear whether the definitions of the receptivity coefficients used in the experimental works are applicable for the case of excitation of low-frequency Görtler vortices, for which the disturbance-source near-field can be very large and the relative role of continuous-spectrum modes can be more significant compared to the previously studied cases of TS and CF waves. Such kind of theoretical analysis and comparison of corresponding numerical results with the experimental data are the main goals of the present investigation.

2 Theoretical and numerical models

2.1 Disturbance equations

The controlled disturbances excited in the boundary layer in the experiment [38] have very low amplitudes (several tenths or even hundredths of a percent of the mean flow velocity). Therefore, we assume that their generation and propagation downstream from the source are described with a good accuracy by linearized equations.

Let us consider a slightly concave plate of infinite span placed under zero angle of attack into a uniform flow of a viscous incompressible fluid with velocity vector of length U_e , which is perpendicular to the plate leading edge. We assume that the radius $R > 0$ of the plate curvature is constant and significantly greater than thickness δ of the boundary layer formed on the plate under the action of viscosity. Let us introduce the following notations: $x \geq 0$ is the stream-wise coordinate (the arc length along the plate surface counted from the leading edge), $y \geq 0$ is the wall-normal coordinate (a distance from the plate surface), z is the span-wise coordinate (along the leading edge of the plate), which is perpendicular to the (x, y) -plane, and t is the time. The flow, which has been established over the plate in the absence of any disturbances, we call the *base flow*. The velocity component of the base flow in the span-wise direction is equal to zero. The velocity components U and V in the x - and y -directions, respectively, and the pressure P does not depend on both z and t .

Let the disturbance source be an oscillating impermeable membrane of stream-wise width l extended infinitely in the z -direction and located downstream of the plate leading edge between coordinates $x_0 - l$ and x_0 , where $x_0 \gg l$. Let us denote the velocity components and the pressure of the perturbed flow by $u(x, y, z, t)$, $v(x, y, z, t)$, $w(x, y, z, t)$ and $p(x, y, z, t)$, respectively. Using the boundary-layer normalization, we scale time by x_0/U_e ; x and l by x_0 ; y, z, R and δ by x_0/\sqrt{Re} ; u by U_e ; v and w by U_e/\sqrt{Re} ; p by $\rho U_e^2/Re$, where $Re = x_0 U_e/\nu$ denotes the Reynolds number (which differs from the one used in the experiment description in Sect. 1), ρ is the fluid density, and ν is the fluid kinematic viscosity. For dimensionless variables, we keep the same notations.

In the considered case, when $R \gg \delta$, the base flow developed over the plate far from its leading edge satisfies the Blasius equations [20,46,51]:

$$U \frac{\partial U}{\partial x} + V \frac{\partial U}{\partial y} = \frac{\partial^2 U}{\partial y^2}, \quad \frac{\partial U}{\partial x} + \frac{\partial V}{\partial y} = 0, \quad (1)$$

with the following no-slip, no-penetration and free-stream boundary conditions:

$$U(x, 0) = V(x, 0) = 0, \quad U(x, \infty) = 1, \quad (2)$$

where, in accordance with the above scaling, $U(x, y)$ and $V(x, y)$ are the dimensionless stream-wise and wall-normal velocities.

The system of linear equations, describing the development of small-amplitude Görtler vortices in the two-dimensional boundary layer, has the following form

$$\begin{aligned} \frac{\partial u'}{\partial t} + U \frac{\partial u'}{\partial x} + \frac{\partial U}{\partial x} u' + V \frac{\partial u'}{\partial y} + \frac{\partial U}{\partial y} v' &= \frac{\partial^2 u'}{\partial y^2} + \frac{\partial^2 u'}{\partial z^2}, \\ \frac{\partial v'}{\partial t} + U \frac{\partial v'}{\partial x} + \frac{\partial V}{\partial x} u' + V \frac{\partial v'}{\partial y} + \frac{\partial V}{\partial y} v' + 2\text{Gö}^2 U u' + \frac{\partial p'}{\partial y} &= \frac{\partial^2 v'}{\partial y^2} + \frac{\partial^2 v'}{\partial z^2}, \\ \frac{\partial w'}{\partial t} + U \frac{\partial w'}{\partial x} + V \frac{\partial w'}{\partial y} + \frac{\partial p'}{\partial z} &= \frac{\partial^2 w'}{\partial y^2} + \frac{\partial^2 w'}{\partial z^2}, \\ \frac{\partial u'}{\partial x} + \frac{\partial v'}{\partial y} + \frac{\partial w'}{\partial z} &= 0, \end{aligned} \quad (3)$$

where $u' = u - U$, $v' = v - V$, $w' = w$, $p' = p - P$, and $\text{Gö} = \sqrt{Re/R}$ is the Görtler number. Note that this Görtler number coincides with the Görtler number Gö introduced in Sect. 1 when the thickness δ of the boundary layer is defined as $\sqrt{x_0 \nu / U_e}$.

This system is derived from the full Navier–Stokes equations for viscous incompressible fluid using linearization and parabolization in the stream-wise direction by dropping viscous terms and the stream-wise derivative of the pressure, which are relatively small in the case of large Reynolds numbers [9,28].

We assume that there are no disturbances of the base flow upstream of the membrane, the no-slip and the no-penetration conditions are satisfied on the plate surface downstream from the membrane, and the disturbances decay to zero as $y \rightarrow \infty$.

The boundary conditions on the membrane surface at $1 - l \leq x \leq 1$ require special consideration. Let the oscillating membrane undergo instantaneous shifts $\xi(x, z, t)$, $\eta(x, z, t)$ and $\zeta(x, z, t)$ about its neutral position along x -, y - and z -axis, respectively. Then the no-slip conditions take the form

$$\begin{aligned} \frac{\partial \xi}{\partial t} &= u(x + \xi, \eta, z + \zeta, t), \\ \frac{\partial \eta}{\partial t} &= v(x + \xi, \eta, z + \zeta, t), \\ \frac{\partial \zeta}{\partial t} &= w(x + \xi, \eta, z + \zeta, t). \end{aligned}$$

Assuming that the displacements and the velocities of points of the membrane surface in the x - and z -directions are negligible, we expand the flow velocity components in the Taylor series near point $(x, 0, z)$, setting $\xi = \zeta = \partial \xi / \partial t = \partial \zeta / \partial t = 0$ and discarding the nonlinear (with respect to η) terms. Generally, the procedure can be misleading as the decision whether the membrane height is small or whether the nonlinear terms are important is dictated by physics (see, e.g., [13]). In the present case, the quite favorable comparison of the numerical and experimental results presented in Sect. 3 substantiates the assumption. Taking then into account that at $y = 0$, the velocity of the base flow satisfies the equalities $U = V = 0$ and $\partial V / \partial y = -\partial U / \partial x = 0$, we get, finally, the following linearized boundary conditions for the disturbance velocities:

$$\begin{aligned} u'(x, 0, z, t) &= -\frac{\partial U}{\partial y}(x, 0)\eta, \\ v'(x, 0, z, t) &= \frac{\partial \eta}{\partial t}, \\ w'(x, 0, z, t) &= 0, \quad 1 - l \leq x \leq 1. \end{aligned}$$

The substantiation of such boundary conditions can be traced to [4] and, hence, they are called sometimes as Benjamin's boundary conditions. They are widely used, in particular, in studying various shear-flow instabilities near compliant coatings [23,34,67] and other surface nonuniformities in both parallel and nonparallel flows [44,60].

We assume that the membrane oscillation is harmonic on z and t , i.e.,

$$\eta(x, z, t) = \text{real} H_{\beta\omega}(x) e^{i(\beta z - \omega t)},$$

where $\beta \neq 0$ and $\omega \geq 0$ are the real span-wise wave-number and angular frequency, respectively, and $H_{\beta\omega}(x)$ is a scalar nonnegative function which is identically equal to zero at $x \leq 1 - l$ and $x \geq 1$ and depends, in general, on β and ω . In this case, the solution of system (3) can be found in the following form

$$\begin{pmatrix} u'(x, y, z, t) \\ v'(x, y, z, t) \\ w'(x, y, z, t) \\ p'(x, y, z, t) \end{pmatrix} = \text{real} \begin{pmatrix} \bar{u}(x, y) \\ \bar{v}(x, y) \\ \bar{w}(x, y) \\ \bar{p}(x, y) \end{pmatrix} e^{i(\beta z - \omega t)}. \quad (4)$$

Then the system (3) is reduced to a system of equations for the complex amplitudes of disturbances and, by using the continuity equation of the base flow, can be rewritten in the following form

$$\begin{aligned} \frac{\partial \bar{u}}{\partial x} + \frac{\partial \bar{v}}{\partial y} + i\beta \bar{w} &= 0, \\ \frac{\partial(U\bar{v} + V\bar{u})}{\partial x} + 2\frac{\partial V\bar{v}}{\partial y} + i\beta V\bar{w} + 2G\ddot{\omega}^2 U\bar{u} + \frac{\partial \bar{p}}{\partial y} &= \frac{\partial^2 \bar{v}}{\partial y^2} - \beta^2 \bar{v} + i\omega \bar{v}, \\ \frac{\partial U\bar{w}}{\partial x} + \frac{\partial V\bar{w}}{\partial y} + i\beta \bar{p} &= \frac{\partial^2 \bar{w}}{\partial y^2} - \beta^2 \bar{w} + i\omega \bar{w}, \\ V\frac{\partial \bar{u}}{\partial y} - \frac{\partial V}{\partial y} \bar{u} + \frac{\partial U}{\partial y} \bar{v} - U\frac{\partial \bar{v}}{\partial y} - i\beta U\bar{w} &= \frac{\partial^2 \bar{u}}{\partial y^2} - \beta^2 \bar{u} + i\omega \bar{u}. \end{aligned} \quad (5)$$

Note that the form of the stream-wise momentum equation [the last equation in (5)] differs from the conventional one, cf., e.g., eq. (3) in [9]. It was obtained by applying the continuity equations for the base flow and disturbances to remove x -derivatives in the stream-wise momentum equation. This modification of the original system is essential for their efficient numerical analysis presented below.

The initial conditions for the system (5) and the boundary conditions at $y = \infty$ have the form

$$\bar{u}(1 - l, y) = \bar{v}(1 - l, y) = \bar{w}(1 - l, y) = 0 \quad (6)$$

and

$$\bar{u}(x, \infty) = \bar{v}(x, \infty) = \bar{w}(x, \infty) = 0, \quad x \geq 1 - l, \quad (7)$$

respectively, and the boundary conditions at $y = 0$ have the form

$$\begin{aligned} \bar{u}(x, 0) &= -\frac{\partial U}{\partial y}(x, 0) H_{\beta\omega}(x), \\ \bar{v}(x, 0) &= -i\omega H_{\beta\omega}(x), \\ \bar{w}(x, 0) &= 0, \quad 1 - l \leq x \leq 1, \end{aligned} \quad (8)$$

and

$$\bar{u}(x, 0) = \bar{v}(x, 0) = \bar{w}(x, 0) = 0, \quad x > 1.$$

Note that the model (5)–(8) is justifiable at large Reynolds numbers: $Re \gg 1/H_{\max}$, where

$$H_{\max} = \max H_{\beta\omega}(x),$$

at small amplitudes of oscillations relative to the boundary-layer thickness: $H_{\max} \ll \delta$, and at the boundary-layer thickness much smaller than the characteristic stream-wise wavelength of the vortex [4]. All these conditions are satisfied in the present study.

Table 1 Magnitudes h_{\max} of membranes' oscillations (μm)

λ_z , mm	$f = 2$	5	8	11	14 Hz
8		30.0 ± 2.0	36.0 ± 2.2	45.0 ± 2.0	48.1 ± 3.7
12	27.6 ± 0.3	30.9 ± 0.6	37.8 ± 0.5	47.2 ± 1.0	51.7 ± 2.3

The kinetic energy of the disturbances (4) per unit area in the (x, z) -plane and the entire thickness of the boundary layer, averaged over time and span-wise coordinate, with the used normalization are proportional to

$$\lim_{T \rightarrow \infty} \lim_{Z \rightarrow \infty} \frac{1}{4ZT} \int_{-T-Z}^T \int_{-Z}^Z \int_0^\infty \left(u'(x, y, z, t)^2 + \frac{v'(x, y, z, t)^2}{Re} + \frac{w'(x, y, z, t)^2}{Re} \right) dy dz dt \quad (9)$$

and, as it is easy to see, are proportional to

$$\int_0^\infty \left(|\bar{u}(x, y)|^2 + \frac{|\bar{v}(x, y)|^2}{Re} + \frac{|\bar{w}(x, y)|^2}{Re} \right) dy.$$

For the sake of brevity, we will further call this function of x the *energy* of the solution of system (5).

2.2 The source

In the experiment of [38], the disturbance source consisted of many round membranes of diameter d ranged in the span-wise direction and oscillating pairwise opposite in phase. They simulated span-wise-periodic surface nonuniformities, which generate in the boundary layer some vortical disturbances with the span-wise wavelength of λ_z .

The membranes oscillated with frequencies $f = 2, 5, 8, 11$ and 14 Hz. Their maximum periodic deflections h_{\max} were less than $52 \mu\text{m}$ in all cases (see Table 1). The dimensionless shapes of oscillations over the membrane surface turned out to be the same (within accuracy of the measurements) *at all frequencies* under study, while the phases of oscillations turned out to be constant. These observations mean that the *instantaneous* dimensionless shapes of the membranes' deflections are the same at any instant and correspond to quasistationary displacements.

Hence, for the theoretical description, it turned to be possible to consider the problem of the membrane deflection in the static formulation. For this problem, at $\varepsilon \ll d$ and $h_{\max}/\varepsilon \lesssim 0.2$ (where ε is the membrane thickness), the approximation of the classical theory of small bending of thin plates is valid. In practice, this approach is used sometimes even up to $h_{\max}/\varepsilon \approx 1$ [17]. Preliminary estimates performed by means of approximations of the measured shape of membrane oscillations by analytical solutions given by the theory have shown that the in-plane tension term plays a negligibly weak role at these particular experimental conditions. Neglecting the in-plane tension of the membrane, the problem has an analytical solution (see, e.g., [61, Chapter III, §16]), which has the following form (in the cylindrical system of coordinates related to the point of symmetry of a membrane)

$$h(r) = h_{\max} \left[1 - \left(\frac{2r}{d} \right)^2 \right]^2. \quad (10)$$

Here r is the current distance from the membrane center. To describe better the experimentally observed shape of oscillations, one can use an infinite series of $(2r/d)^{2n}$ (see [61, Chapter XIII, §98]). The formula (10) can be interpreted as the truncation of the series at $n = 2$. Taking into account the first four terms of such an expansion, one can get the formula

$$h(r) = h_{\max} \sum_{n=0}^3 c_n \left(\frac{2r}{d} \right)^{2n}, \quad |r| \leq d/2, \quad (11)$$

where

$$\sum_{n=0}^3 c_n = \sum_{n=1}^3 n c_n = 0,$$

which is in a very good agreement with the measurements for the two used membrane types. The corresponding independent coefficients of (11) are: $c_2 = 1.9375$, -0.3101 and $c_3 = -0.4591$, 0.6534 for the membranes with span-wise periods $\lambda_z = 8$ and 12 mm, respectively.

Assuming the number of the membranes infinite, the span-wise wave-number spectra of both the surface nonuniformities and the vortices are discrete and consist predominantly of a pair of harmonics with wave-numbers $\beta_{\pm n} = \pm 2n\pi/\lambda_z$, where n is positive integer. In all regimes, the amplitudes of first harmonics ($n = 1$) were about 5 times higher than the amplitudes of second ones ($n = 2$) and more than 20 times higher than the amplitudes of other harmonics. Note that as the phase of oscillation of every membrane is constant over its surface, it is possible to provide the real-valued amplitudes h_β of the membrane oscillations at the span-wise wave-number $\beta = \beta_{\pm 1}$ by choosing the initial time instant.

Accordingly, for the disturbance equations described in Sect. 2.1, we will assume

$$H_{\beta\omega}(x) = h_\beta \left(\frac{x-1+l/2}{l} d \right), \quad 1-l \leq x \leq 1.$$

2.3 Numerical model

To discretize the system (5) with the initial conditions (6) and boundary conditions (7) and (8), we use the method of collocations in y -direction. Let us take a sufficiently large $y_{\max} \gg \delta$ and replace the boundary conditions (7) by

$$\bar{u}(x, y_{\max}) = \bar{v}(x, y_{\max}) = \bar{w}(x, y_{\max}) = 0, \quad x > 1-l.$$

The adequacy of the choice of y_{\max} will be analyzed *a posteriori* by the independence (within the specified accuracy) of the obtained results, as y_{\max} is increased.

Let us make the following change of variables in eqs (5)

$$y = y(s) = y_{\max} \frac{1+s}{2+(1-s)\sigma}, \quad -1 \leq s \leq 1, \quad (12)$$

where $\sigma > 0$ is the scaling factor, and replace \bar{p} , \bar{u} , \bar{v} , and \bar{w} by interpolation polynomials using the nodes

$$s_j = \cos \frac{\pi j}{N+1}, \quad j = 1, \dots, N, \quad (13)$$

to interpolate the pressure in s and the same points and $s_0 = 1$ and $s_{N+1} = -1$ to interpolate the velocity components. Requiring fulfillment of the obtained equations at points (13), and using the methods described in [64] for computing the derivatives of the interpolation polynomials, we come to a system of ordinary differential and algebraic equations of the form

$$v(1-l) = 0, \quad \frac{d}{dx} D(x)v = J(x)v + Gp + H(x)f_v(x), \quad F(x)v + H(x)f_p(x) = 0, \quad (14)$$

with a scalar function $H(x) = H_{\beta\omega}(x)$ such that

$$H(1-l) = H(x) \equiv 0, \quad x \geq 1. \quad (15)$$

where $v(x) \in \mathbf{C}^{n_v}$ and $p(x) \in \mathbf{C}^{n_p}$ are the vectors of values of the velocity components and pressure, respectively, at the internal nodes of the grid, $J(x) \in \mathbf{C}^{n_v \times n_v}$ and $F(x) \in \mathbf{C}^{n_p \times n_v}$ are matrices, and $f_v(x) \in \mathbf{C}^{n_v}$, $f_p(x) \in \mathbf{C}^{n_p}$ are vectors dependent smoothly on x , $n_v = 3N$, $n_p = N$, and $G \in \mathbf{C}^{n_v \times n_p}$ is a matrix that is independent of x .

Note that the first equality in (14) represents the initial condition (6), the second one approximates the first three equations in (5), and the third one approximates the fourth equation in (5). The boundary conditions (8) are represented by the terms $H(x)f_v(x)$ and $H(x)f_p(x)$.

Taking into account that $l \ll 1$ (due to assumption $x_0 \gg l$ in Sect. 2.1), we consider further the base flow to be constant in the range of $1 - l \leq x \leq 1$, assuming

$$\begin{aligned} D(x) &\equiv D(1), & J(x) &\equiv J(1), & F(x) &\equiv F(1), \\ f_v(x) &\equiv f_v(1), & f_p(x) &\equiv f_p(1), & 1 - l &\leq x \leq 1. \end{aligned} \quad (16)$$

For the system of differential-algebraic equations (14), which is a discrete version of system (5), the energy of the solution is

$$\mathcal{E}(v(x)) = (Ev(x), v(x)),$$

where $(., .)$ means the complex Euclidean scalar product,

$$E = \text{diag}(K, K/Re, K/Re),$$

K is a diagonal matrix of the Gauss–Lobatto quadrature weights [12] multiplied by the values of Jacobian of the transformation (12) at nodes (13).

The matrices $D(x)$, $J(x)$ and $F(x)$ include the base-flow velocities U and V and their derivatives with respect to y at grid nodes $y(s_j)$. We compute $U(x, y(s_j))$ and $V(x, y(s_j))$ for $x = 1$ and then use these values as initial conditions for computing U and V at the grid nodes for $x > 1$ by the delaying coefficients method and the Crank–Nicolson scheme [58].

For computing $U(1, y(s_j))$ and $V(1, y(s_j))$, we need to solve the system (1), (2). Its solution can be represented in the self-similar form [51]:

$$U = \frac{dg}{dr}, \quad V = \frac{1}{2\sqrt{x}}(rU - g),$$

where g is a function of the similarity variable $r = y/\sqrt{x}$, which satisfies the equation

$$2\frac{d^3g}{dr^3} + g\frac{d^2g}{dr^2} = 0$$

with the boundary conditions

$$g(0) = \frac{dg}{dr}(0) = 0, \quad \frac{dg}{dr}(\infty) = 1.$$

For computing g at the nodes $r_j = y(s_j)$, we use the method described in detail in [42, 54].

Applying an algebraic dimension reduction proposed in [10, 47] to the differential-algebraic initial-value problem (14)–(16) with the matrices and right-hand side, smoothly dependent on x , one can show that the following conditions

$$\det D(x) \neq 0, \quad \det F(x)D(x)^{-1}G \neq 0 \quad (17)$$

guaranty the existence and uniqueness of the solution and make it possible to eliminate p in (14). Taking this into account, we will consider separately the generation of disturbances by solving the initial-value problem

$$\begin{aligned} v(1-l) &= 0, & \frac{d}{dx}D(1)v &= J(1)v + Gp + H(x)f_v(1), \\ F(1)v + H(x)f_p(1) &= 0, & 1-l < x &\leq 1, \end{aligned} \quad (18)$$

and the downstream propagation of disturbances $v^0 = v(1)$ generated by (18), solving the initial-value problem

$$v(1) = v^0, \quad \frac{d}{dx}D(x)v = J(x)v + Gp, \quad F(x)v = 0, \quad x > 1. \quad (19)$$

For approximating these initial-value problems in x , we will use the BDF2 method [26] with fixed grid steps.

In addition, we will use the adjoint initial-value problem

$$\tilde{v}(1) = \tilde{v}^0, \quad -D(1)^*\frac{d\tilde{v}}{dx} = J(1)^*\tilde{v} + F(1)^*\tilde{p}, \quad G^*\tilde{v} = 0, \quad 1 > x \geq 1-l,$$

where I is the identity matrix of order n_v and $*$ denotes the conjugate transposition. The adjoint problem is solved backwards in x with a given initial vector \tilde{v}^0 satisfying $G^*\tilde{v}^0 = 0$. One can prove that the solution of (18) satisfies the equality

$$(D(1)v(1), \tilde{v}^0) = \int_{1-l}^1 H_c(x)^* H(x) dx,$$

where

$$H_c(x) = (\tilde{v}(x), f_v(1)) + (\tilde{p}(x), f_p(1)).$$

Choosing the initial vector for the adjoint problem as

$$\tilde{v}^0 = [I - G(YG)^{-1}Y]^* D(1)^{-*} u,$$

where $Y = F(1)D(1)^{-1}$ and u is a given arbitrary n_v -component vector, we obtain

$$(v(1), u) = (D(1)v(1), \tilde{v}^0) = \int_{1-l}^1 H_c(x)^* H(x) dx.$$

The function $H_c(x)$ will be referred to as *the adjoint source amplitude* corresponding to u .

Any solution $v(x)$ of the initial-value problem (19) can be represented in the following form:

$$v(x) = S(x)v^0,$$

where $S(x) \in \mathbf{C}^{n_v \times n_v}$ is a matrix of fundamental solutions. Since $v^0 = S(1)v^0$ for any vector v^0 , satisfying the condition $F(1)v^0 = 0$, the matrix $S(1)$ has to be a projector onto $\ker F(1)$. For instance, we can choose $S(1) = Q$, where

$$Q = I - F(1)^*(F(1)F(1)^*)^{-1}F(1)$$

is the orthogonal projector onto $\ker F(1)$. If $S(1)$ is fixed, then matrix $S(x)$ is unique and can be obtained column-by-column by solving the initial-value problem (19) with the initial vectors v^0 equal to columns of $S(1)$.

The computations to be described below were performed for the following values of parameters: $y_{\max} = 30$, $\sigma = 11$, the number $N = 50$ of grid points in y -direction, the number of grid points on the source in x -direction and from $x = 1$ to $x = 4.4$ was chosen to be 2000 and 500, respectively. Reducing the steps of grids and increasing y_{\max} did not lead to any visible changes in the results. The parameters of computations are given in Tables 2 and 3.

Table 2 Parameters of computations for the membrane with $\lambda_z = 8$ mm ($\Lambda = 152$)

f , Hz	5	8	11	14
H_{\max}	0.0421	0.0507	0.0632	0.0677
Gö	3.6278	3.6332	3.6288	3.6308
β	0.5217	0.5202	0.5214	0.5209
ω	0.9257	1.4812	2.0366	2.5921
$Re \times 10^{-5}$	1.6583	1.6682	1.6601	1.6638
l	0.0135	0.0135	0.0135	0.0135

Table 3 Parameters of computations for the membrane with $\lambda_z = 12$ mm ($\Lambda = 280$)

f , Hz	2	5	8	11	14
H_{\max}	0.0426	0.0478	0.0584	0.0730	0.0800
Gö	3.6427	3.6430	3.6430	3.6429	3.6428
β	0.3472	0.3472	0.3472	0.3472	0.3472
ω	0.3715	0.9288	1.4861	2.0433	2.6006
$Re \times 10^{-5}$	1.6747	1.6752	1.6752	1.6751	1.6749
l	0.0200	0.0200	0.0200	0.0200	0.0200

3 Spectral content of Görtler vortices and the receptivity coefficients

The receptivity coefficient can be defined by analogy with the case of TS wave excitation as a constant $C_{\lambda_z, f}$ which is independent of the source amplitude and which gives an approximation of the following form for a disturbance generated by a source located at $x = 1$:

$$v(x) \approx C_{\lambda_z, f} v_m(x) \int_{-\infty}^{\infty} H(\xi + 1) e^{-i\alpha_{mr}\xi} d\xi, \quad x \gg 1, \quad (20)$$

where $v_m(x)$ is the solution of the initial-value problem (19) with v^0 being the leading local mode at $x = 1$, and α_{mr} is the real part of eigenvalue corresponding to v^0 . This approximation is based on the observation that to obtain the downstream propagation of a disturbance with account of a nonparallelism of the boundary-layer streamlines, it is necessary to solve the initial-value problem (19), as, for example, in [15], rather than to use the so-called N -factor approach based on pure local analysis. The right-hand side of (20) at $x = 1$ can be treated as the initial amplitude generated due to a resonance effect.

The receptivity coefficient $C_{\lambda_z, f}$ can be estimated using (20) and data on the complete disturbance velocity $v(x)$ obtained numerically or experimentally with a specific source. However, in this case, there is no confidence that it is independent of the amplitude $H(x)$ of the source.

In this section, we propose and justify an approach for finding approximations of type (20) with the receptivity coefficients, which can be estimated independently of the source amplitude. The most obvious way to obtain such an approximation is based on the adjoint function corresponding to the leading local mode. However, as we show below, in the case of Görtler vortices, this approach gives a wrong value of the receptivity coefficient due to the nonparallelism of the boundary-layer streamlines.

We propose to solve the above problem by using the so-called optimal disturbances. Despite the fact that near the disturbance source and over the majority of the stream-wise region the optimal disturbance is a tiny fraction of the roughness-induced disturbance hardly observable in a laboratory experiment, it can be a useful numerical tool when it is combined with the adjoint-function approach. In particular, it is shown that the extracted optimal parts of the initial disturbances under consideration make it possible to explain their far-field linear propagation and to define physically meaningful coefficients of the boundary-layer receptivity to surface nonuniformities at excitation of Görtler vortices.

3.1 The receptivity coefficients via optimal disturbances

Let us consider the stream-wise development of disturbances from the point $x = 1$ by solving the initial-value problem (19). Let $x_0 > 1$ denote a point at which the disturbances are observed.

A solution $v(x) = v_{\text{opt}}(x)$ of the initial-value problem (19) with the unitary energy at $x = 1$ is called the *optimal disturbance*, if

$$\mathcal{E}(v_{\text{opt}}(x_0)) = \max \{ \mathcal{E}(S(x_0)u) : \mathcal{E}(u) = 1, \quad F(1)u = 0 \},$$

where $S(x)$ is the matrix of fundamental solutions introduced in Sect. 2.3. Among all solutions of the initial-value problem with the unitary energy at $x = 1$, such a solution has a maximum energy at $x = x_0$.

The optimal disturbance $v_{\text{opt}}(x)$ can be computed solving the initial-value problem (19) with the initial value $v^0 = E^{-1/2}\eta$, where η is a normalized right singular vector of the matrix

$$E^{1/2}S(x_0)E^{-1/2}P$$

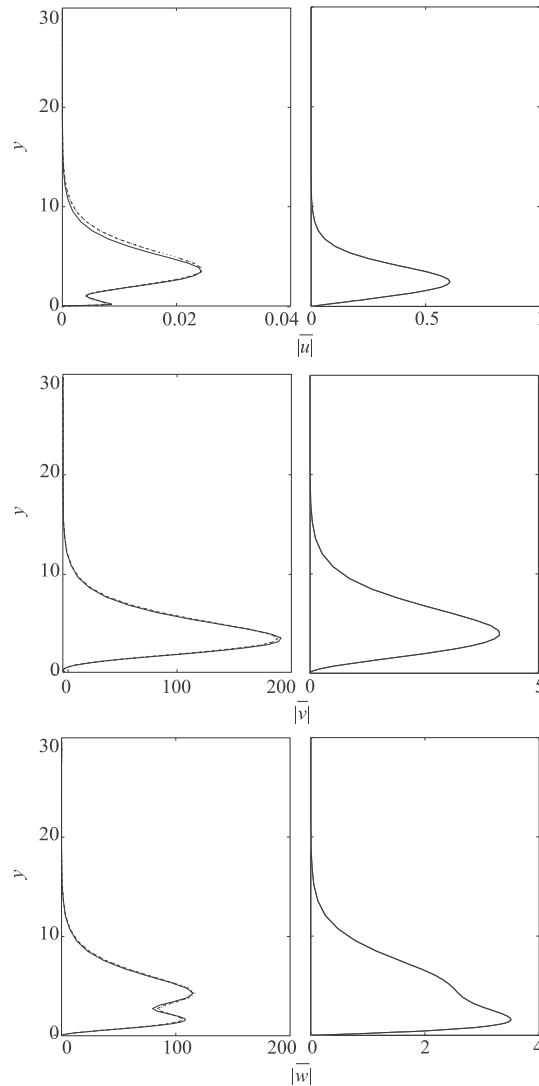


Fig. 1 Wall-normal profiles of magnitudes of three velocity components at $x = 1$ for three optimal disturbances with $x_0 = 3$ (solid lines), 4.5 (dashed lines) and 6 (dotted lines), (left), and those for the leading local mode (right) in the cases of $\lambda_z = 8$ mm and $f = 8$ Hz

corresponding to its maximum singular value, and P is the orthogonal projector onto $\ker F(1)E^{-1/2}$. The matrix $S(x_0)$, required to form the above matrix, can be computed as described in Sect. 2.3. The maximum singular value in the present case is simple. Therefore, the corresponding normalized right singular vector η is unique up to a multiplicative constant of unitary magnitude. Hence, the optimal disturbance is unique up to a multiplicative constant of unitary magnitude as well. To obtain the complete uniqueness, we normalize $v_{\text{opt}}(x)$ to make the stream-wise velocity component of $v_{\text{opt}}(1)$ positive at the point of its maximum magnitude in the wall-normal profile.

Figure 1 (left) shows magnitudes of three velocity components of the optimal disturbance at $x = 1$ for three different values of x_0 . The data are presented for the case of $\lambda_z = 8$ mm and $f = 8$ Hz, the results obtained for other values of λ_z and f being quite similar. It is seen that the velocities have quite smooth wall-normal profiles and weakly depend on x_0 . Note that the wall-normal and span-wise velocities have an additional scaling, being multiplied by $\sqrt{Re} \approx 408$ (see Tables 2, 3), in contrast to the stream-wise velocity. Thus, both the scaled and the dimensional stream-wise velocities are significantly smaller than the others are. Hence, similarly to optimal disturbances in channels and flat-plate boundary layer (see, e.g., review in [7]), the optimal disturbances in the concave plate boundary layer can be interpreted as a system of counter-rotating stream-wise vortices, evolving downstream, however, into the Görtler vortices rather than into stream-wise streaks.

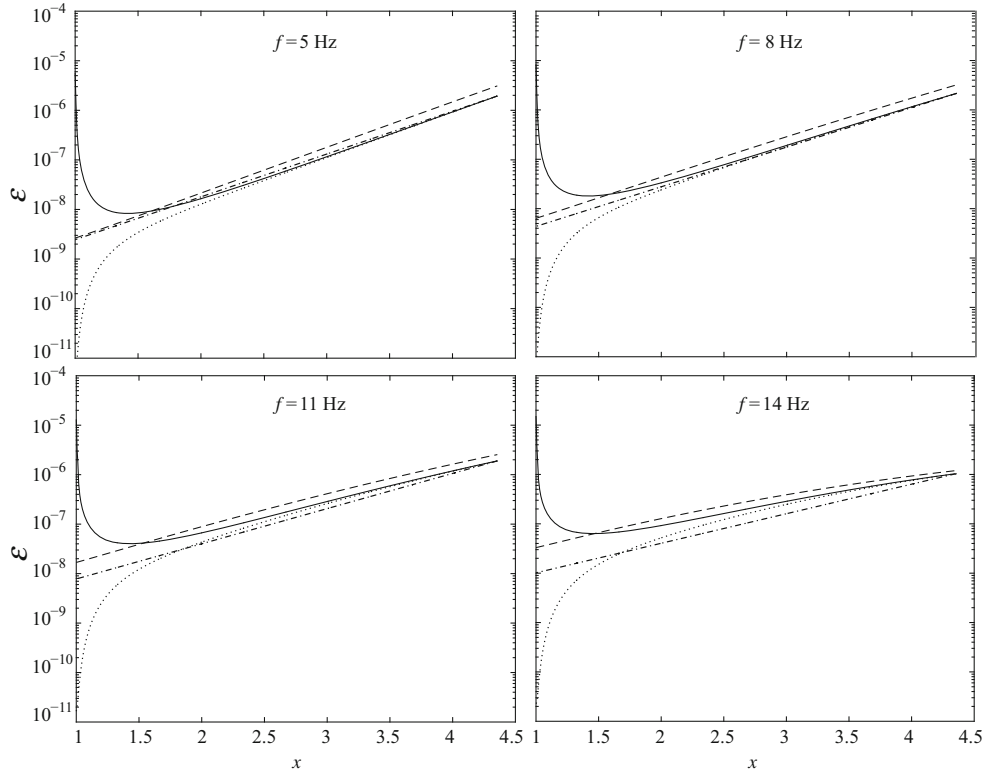


Fig. 2 Comparison of stream-wise distributions of energy of total disturbance (*solid lines*), its optimal part (*dotted lines*) and its modal part (*dashed lines*) and an estimated energy growth (*dash-dotted lines*) using (32) for various frequencies and $\lambda_z = 8$ mm

Let us represent any solution $v(x)$ of problem (19) as

$$v(x) = \kappa v_{\text{opt}}(x) + v_r(x), \quad (21)$$

choosing $\kappa = (Ev(1), v_{\text{opt}}(1))$ to provide $(Ev_r(1), v_{\text{opt}}(1)) = 0$. By definition, $v_{\text{opt}}(x)$ and $v_r(x)$ are mutually E -orthogonal at $x = 1$, and as one can prove, at $x = x_0$. Therefore,

$$\mathcal{E}(v(x)) = \mathcal{E}(\kappa v_{\text{opt}}(x)) + \mathcal{E}(v_r(x)), \quad x = 1, x_0.$$

The stream-wise distributions of energy of both the total disturbance $v(x)$ and its optimal part (i.e., the first term in (21)) are shown in Figs. 2 and 3 for various values of frequency f at $\lambda_z = 8$ and 12 mm, respectively. It is observed that the optimal part $\kappa v_{\text{opt}}(x)$ of the total disturbance $v(x)$ is relatively small at $x = 1$, i.e., $v(1)$ and $v_{\text{opt}}(1)$ are almost orthogonal. However, when $x \gg 1$ the remainder $v_r(x)$ becomes negligible and

$$v(x) \approx \kappa v_{\text{opt}}(x), \quad x \gg 1, \quad (22)$$

i.e., $v(x)$ and $v_{\text{opt}}(x)$ at $x \gg 1$ are almost collinear. Thus, despite the disturbance generated in the vicinity of the surface nonuniformities is far from $\kappa v_{\text{opt}}(x)$, it is its optimal part that forms a corresponding Görtler vortex at $x \gg 1$. In the other words, when the surface nonuniformities generate disturbances, solely their optimal parts transform to observable disturbances at $x \gg 1$. The remainders vanish at $x \gg 1$. Thus, the efficiency of source can be estimated by the ratio $\mathcal{E}(\kappa v_{\text{opt}}(1))/\mathcal{E}(v(1))$. If this ratio equals to 1, i.e., the source generates only optimal disturbances, it is the most efficient. The source used in the considered experiment, as presumably any surface nonuniformity, is not too efficient at excitation of the disturbances in shear flows.

The coefficient κ in (22) can be represented as

$$\kappa = \int_{1-l}^1 H_0(\xi)^* H(\xi) d\xi, \quad (23)$$

where $H_0(x)$ is the adjoint source amplitude corresponding to $Ev_{\text{opt}}(1)$.

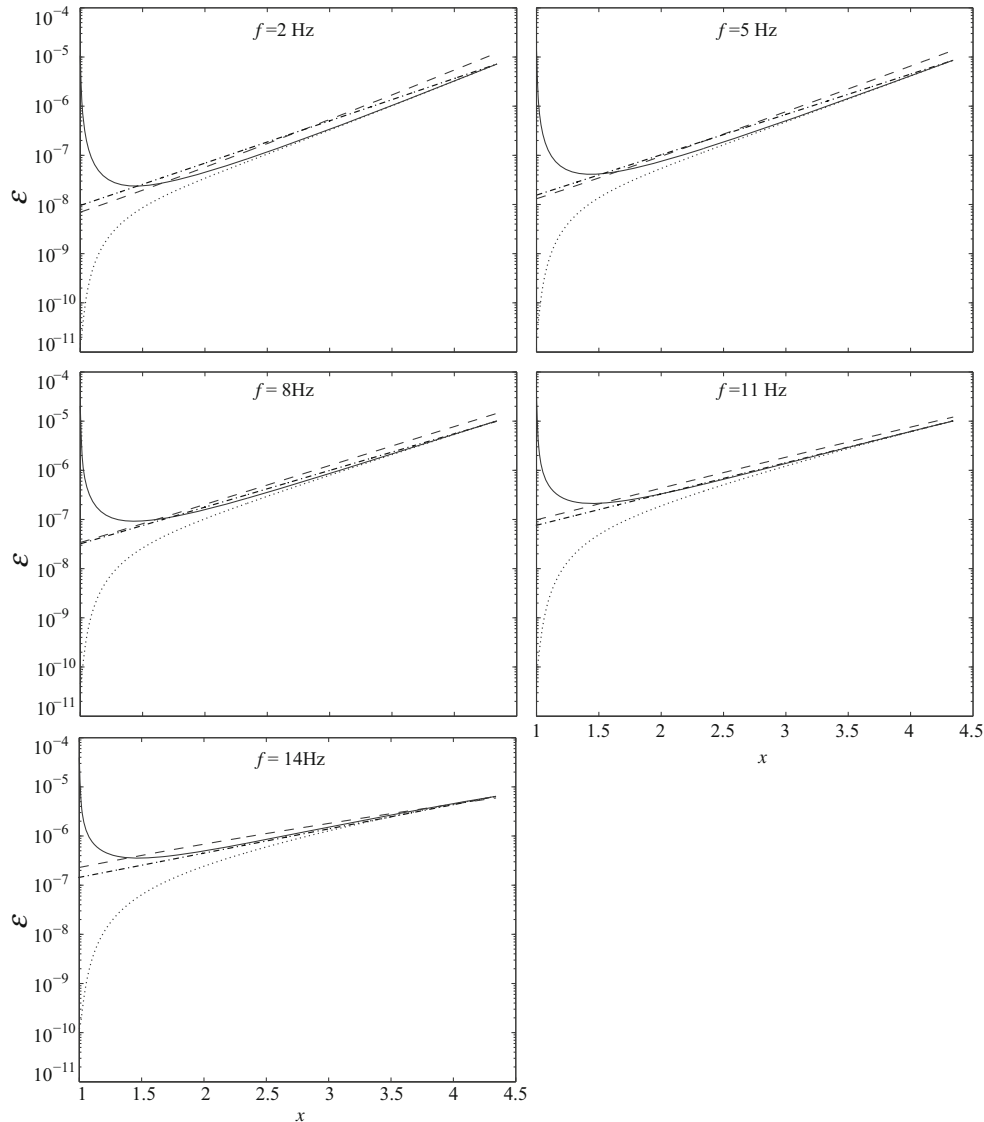


Fig. 3 Comparison of stream-wise distributions of energy of total disturbance (*solid lines*), its optimal part (*dotted lines*) and its modal part (*dashed lines*) and an estimated energy growth (*dash-dotted lines*) using (32) for various frequencies and $\lambda_z = 12$ mm

It appeared that the magnitudes $|H_o(x)|$ and phases $\arg(H_o(x))$ of the adjoint source amplitudes $H_o(x)$ for all cases considered in the paper are almost constant along the stream-wise coordinate. This enables us to replace formula (23) by the approximate one

$$\kappa \approx \hat{\kappa} = H_o(1 - l/2)^* \int_{1-l}^1 H(\xi) d\xi. \quad (24)$$

A direct computation showed that the resulting relative error $|\hat{\kappa} - \kappa|/|\kappa|$ for all considered values of λ_z and f is not larger than $1.3 \cdot 10^{-3}$.

Function $C_{\lambda_z, f}^0 = H_o(1 - l/2)^*$ can be regarded as the *coefficient of receptivity* of the boundary layer over a concave wall to surface nonuniformities at excitation of the Görtler vortices. On computing the optimal disturbance $v_{\text{opt}}(x)$ and the receptivity coefficient, we can find immediately (by means of formulae (22), (24)) an approximate value of the disturbance amplitude generated by the source as

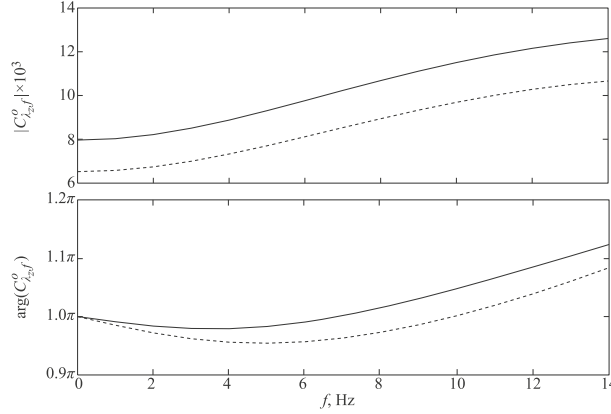


Fig. 4 Magnitudes (*top*) and phases (*bottom*) of receptivity coefficients $C_{\lambda_z, f}^0$ for $\lambda_z = 8$ (*dashed lines*) and 12 mm (*solid lines*)

$$v(x) \approx C_{\lambda_z, f}^0 v_{\text{opt}}(x) \int_{1-l}^1 H(\xi) d\xi, \quad x \gg 1, \quad (25)$$

for any particular amplitude $H(x)$ of the source.

The magnitudes $|C_{\lambda_z, f}^0|$ and the phases $\arg(C_{\lambda_z, f}^0)$ of the computed receptivity coefficients $C_{\lambda_z, f}^0$ are presented in Fig. 4 versus the disturbance frequency for two values of the span-wise wavelength λ_z . It is seen that both the receptivity magnitudes and phases increase, in general, with λ_z and f (excluding receptivity phases at frequencies below 5 Hz).

Note that all computations with the optimal disturbances are very stable numerically because they are based on the singular value decomposition, which is one of the most precise procedures of the matrix analysis. Particularly, we compute $C_{\lambda_z, f}^0$ with a relative accuracy higher than 10^{-10} and the almost orthogonality of the total and optimal disturbances is not an obstacle in the present numerical approach.

3.2 Modal approach

Let us consider now the generalized eigenvalue problem

$$i\alpha D(1)\chi = J(1)\chi + G\mu, \quad F(1)\chi = 0,$$

corresponding to the initial-value problems (18) and (19) at $x = 1$. Here α is an eigenvalue and χ is the velocity part of corresponding eigenvector. Since we are interested further only in the velocity parts of eigenvectors, we will use for simplicity the term ‘eigenvector’ for χ .

Let us denote the eigenvalue with the minimal imaginary part by α_m and some corresponding eigenvector by v_m^0 . In the considered case, the eigenvalue α_m is simple, and therefore, the above eigenvector is unique up to a multiplicative constant. Let us now choose this constant such that $\mathcal{E}(v_m^0) = 1$ and the stream-wise velocity of v_m^0 is positive at the point of its maximum magnitude in the wall-normal profile. The eigenvector v_m^0 will be referred to as the *leading local mode* of the initial-value problems (18) and (19) at $x = 1$.

Figure 1 (*right*) shows magnitudes of three velocity components of the leading local mode at $x = 1$. Their scaling is the same as in Fig. 1 (*left*). It is seen that all components have smooth wall-normal profiles, and in contrast to the dimensional stream-wise velocity of the optimal disturbance, the corresponding velocity of the leading local mode is significantly larger than two other dimensional velocities.

Denote by \tilde{v}_m^0 the eigenvector of the adjoint generalized eigenvalue problem

$$-i\alpha D(1)^* \tilde{\chi} = J(1)^* \tilde{\chi} + F(1)^* \tilde{\mu}, \quad G^* \tilde{\chi} = 0,$$

corresponding to the eigenvalue α_m^* and normalized such that $(D(1)v_m^0, \tilde{v}_m^0) = 1$. The eigenvector \tilde{v}_m^0 will be referred to as the *adjoint leading local mode* of the initial-value problems (18) and (19) at $x = 1$.

The initial vector of the initial-value problem (19) can be represented as

$$v^0 = \rho v_m^0 + v_{rm}^0, \quad (26)$$

where $\rho = (D(1)v^0, \tilde{v}_m^0)$, and therefore, $(D(1)v_{rm}^0, \tilde{v}_m^0) = 0$. The coefficient ρ in (26) can be represented as

$$\rho = \int_{1-l}^1 H_m(\xi)^* H(\xi) d\xi, \quad (27)$$

where $H_m(x)$ means the adjoint source amplitude corresponding to $D(1)^* \tilde{v}_m^0$.

Similar to the case of the adjoint source amplitude $H_o(x)$, the values of $H_m(x)$ appeared to be almost constant. This enables us to replace again formula (27) by the approximate one

$$\rho \approx \hat{\rho} = H_m(1-l/2)^* \int_{1-l}^1 H(\xi) d\xi.$$

A direct computation shows that the resulting relative error $|\hat{\rho} - \rho|/|\rho|$ for all considered values of λ_z and f is not larger than $9.2 \cdot 10^{-5}$.

By virtue of (26), the solution of the initial-value problem (19) can be represented as

$$v(x) = \rho v_m(x) + v_{rm}(x), \quad (28)$$

where $v_*(x) = S(x)v_*^{(0)}$ ('*' means 'm' or 'mr') is the solution of the initial-value problem (19) with the initial vector $v^0 = v_*^0$. It would seem that for $x \gg 1$ the first term in the right-hand side of (28) coincides with a good accuracy with $v(x)$. However, this is not quite so. This point is illustrated in Figs. 2 and 3 where the contribution of the leading mode, i.e., $\mathcal{E}(\rho v_m(x))$ is shown (dashed lines) alongside with the energy of the total disturbance (solid lines) and its optimal part (dotted lines). While apparently, the growth rates (i.e., tangents of the growth curves) of the modal and optimal parts approach the growth rate of the total disturbance concurrently, there is a significant gap at low frequencies between the total disturbance and its modal part in the point of observation. It turns out that this difference can be almost completely eliminated by multiplying $\rho v_m(x)$ by a scalar factor $T_{\lambda_z, f}$. In the capacity of such factor, we can use, for example, a ratio of absolute values of the stream-wise velocity of the total disturbance (taken in the observation point $x = x_o$ at amplitude maximum in the wall-normal profiles) and the corresponding modal part.

By analogy with the previous section, the value of $C_{\lambda_z, f}^m = T_{\lambda_z, f} H_m(1-l/2)^*$ can be interpreted as a receptivity coefficient of the boundary layer over the concave plate to surface nonuniformities at excitation of Görtler vortices. Computing the leading mode $v_m(x)$ and the receptivity coefficient $C_{\lambda_z, f}^m$, we can find an approximate value of disturbance $v(x)$ generated by the source by means of the formula

$$v(x) \approx C_{\lambda_z, f}^m v_m(x) \int_{1-l}^1 H(\xi) d\xi, \quad x \gg 1, \quad (29)$$

which is similar to formula (25).

In contrast to the receptivity coefficient $C_{\lambda_z, f}^o$, the modal receptivity coefficient $C_{\lambda_z, f}^m$ does not depend only on the adjoint source amplitude, but includes a correction factor $T_{\lambda_z, f}$, for the computation of which one needs to know the value of the total disturbance $v(x)$ at the point of observation that would seem that formula (29) is useless. However, this is not so.

In the decomposition

$$v_m(x) = \pi v_{opt}(x) + v_{ro}(x), \quad \pi = (E v_m(1), v_{opt}(1)),$$

it appears that the first term dominates at $x \gg 1$. Thus, by virtue of equations (25) and (29), the modal receptivity coefficient $C_{\lambda_z, f}^m$ can be computed by the formula

$$C_{\lambda_z, f}^m \approx C_{\lambda_z, f}^o / \pi, \quad (30)$$

which is independent of the value of the total disturbance $v(x)$ at the point of observation.

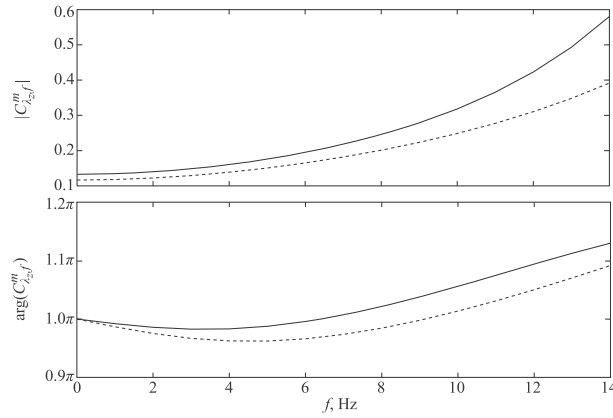


Fig. 5 Magnitudes (*top*) and phases (*bottom*) of modal receptivity coefficients $C_{\lambda_z, f}^m$, computed by formula (30) for $\lambda_z = 8$ (*dashed lines*) and 12 mm (*solid lines*)

Hence, computing the function $v_m(x)$ and the modal receptivity coefficient $C_{\lambda_z, f}^m$ by formula (30), we immediately find an approximate value of the disturbance $v(x)$ generated with a particular source characterized by $H(x)$ by formula (29).

Figure 5 shows that the magnitude $|C_{\lambda_z, f}^m|$ and the phase $\arg(C_{\lambda_z, f}^m)$ of the modal receptivity coefficient $C_{\lambda_z, f}^m$ increase with the λ_z and f (excluding receptivity phases at frequencies below 5 Hz).

3.3 Comparison of numerically and experimentally obtained receptivity coefficients

To compare the modal receptivity coefficients with experimental ones, let us define the latter in terms of the previous sections with account of procedure used in experimental works [36–38] and a great number of previous investigations (see, e.g., a review in [41]). In a general case of fixed base-flow characteristics, model geometry, λ_z and f , the complex-valued receptivity coefficient is defined as the ratio

$$G_{\lambda_z, f} = \frac{B_{\lambda_z, f}}{W_{\lambda_z, f}} \quad (31)$$

of two values: the complex-valued amplitude $B_{\lambda_z, f}$ of the excited boundary-layer instability mode at the location of the source and the complex-valued amplitude $W_{\lambda_z, f}$ of surface vibrations, which is the resonant one to the instability mode. In other words, for our case the resonant spectrum of surface vibrations is defined as the components of the three-dimensional frequency–wave-number spectrum of vibrations selected only for the stream-wise wave-numbers yielded by the dispersion relation for the nonstationary Görtler vortices of the leading discrete spectrum mode.

The magnitude $|G_{\lambda_z, f}|$ of the receptivity coefficient $G_{\lambda_z, f}$ describes the efficiency of production of the Görtler vortices by surface nonuniformities. The phase $\arg(G_{\lambda_z, f})$ defines the phase delay between the displacement of the surface during oscillations and the stream-wise-velocity oscillations within the excited vortices. The disturbance source simulates the span-wise-periodic surface nonuniformities, which lead to the production of an unstable disturbance with a span-wise wavelength of λ_z in the boundary layer. As a result, the spectrum of the simulated nonuniformities and the spectrum of the boundary-layer perturbations are both discrete over the span-wise wave-number β , and for the system of oscillating Görtler vortices produced in the flow, those spectra consist predominantly of a pair of harmonics with wave-numbers $\pm\beta_1$. It is for those wave-numbers the values of the receptivity coefficients are obtained in the present study.

Following the above procedure and assuming that the source is located at $x = 1$, we have

$$W_{\lambda_z, f} = \frac{1}{\gamma} \int_{-\infty}^{\infty} H(\xi + 1) e^{-i\alpha_{mr}\xi} d\xi,$$

where α_{mr} denotes the real part of eigenvalue α_m corresponding to the leading local mode $v_m(1) = v_m^{(0)}$ defined in the previous section, the constant $\gamma = 0.00725$ provides a normalization of the source amplitude applied in experimental works [36–38], and

$$B_{\lambda_z, f} = c\bar{u}_m(1),$$

where $\bar{u}_m(x)$ means the stream-wise velocity of the leading mode $v_m(x)$ at a wall-normal distance corresponding to $U/U_e = 0.6$ and the complex coefficient c is a solution of the least square problem:

$$\sum_{j=1}^p |c\bar{u}_m(x_j) - \bar{u}(x_j)|^2 \rightarrow \min,$$

where $\bar{u}(x)$ means the stream-wise velocity of the disturbance $v(x)$ at a wall-normal distance corresponding to $U/U_e = 0.6$ and x_1, \dots, x_p denote points in x -direction where this disturbance velocity is measured.

Using (29), the constant c can be estimated as

$$c \approx C_{\lambda_z, f}^m \int_{1-l}^1 H(\xi) d\xi.$$

The computations indicate that if $0 \leq f \leq 14$ Hz, then $0 \leq \alpha_{mr} \leq 3.51$ and $0 \leq \alpha_{mr} \leq 3.58$ for $\lambda_z = 8$ mm and 12 mm, respectively. Therefore, $\alpha_{mr}l \ll 1$ (see Tables 2, 3 for corresponding values of l). As $H(\xi + 1) = 0$ when $\xi \leq -l$ or $\xi \geq 0$, it follows that

$$W_{\lambda_z, f} \approx \frac{1}{\gamma} \int_{1-l}^1 H(\xi) d\xi.$$

Thus, the receptivity coefficient $G_{\lambda_z, f}$ can be estimated theoretically via the modal receptivity coefficient $C_{\lambda_z, f}^m$ with the formula

$$G_{\lambda_z, f} \approx \gamma C_{\lambda_z, f}^m \bar{u}_m(1).$$

Shown in Fig. 6 is the comparison of experimental (black symbols) and theoretical (open symbols and lines) distributions of the receptivity coefficients versus frequency f obtained for the span-wise wavelengths $\lambda_z = 8$ and 12 mm. In addition, an extrapolation of the experimentally obtained coefficients to zero frequency using the technique of [37] is marked by crosses. It is seen that the values of the receptivity coefficients, the character and rate of their growth with frequency, as well as the dependence on the span-wise wavelength, are

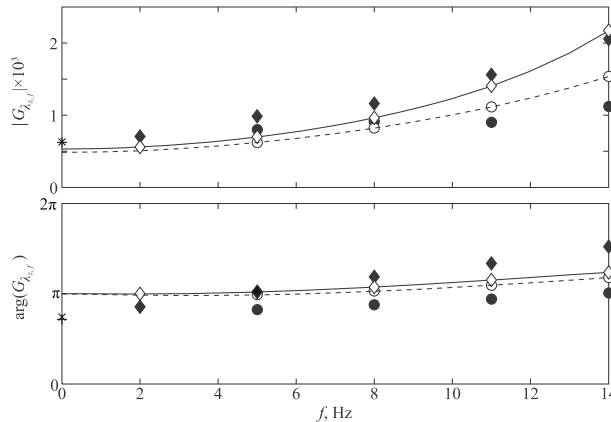


Fig. 6 Comparison of experimental (closed symbols) and computed (open symbols, lines) receptivity coefficients versus frequency for span-wise wavelengths $\lambda_z = 8$ mm (open circle, filled circle, dashed lines) and 12 mm (open diamond, filled diamond, solid lines). Additionally, extrapolation of experimental data to zero frequency is shown for $\lambda_z = 8$ mm (+) and 12 mm (x), respectively

practically the same in the experimental and model cases, although the quantitative values of the receptivity amplitudes and phases are somewhat different. However, taking into account the great complexity of the procedures of determination of these coefficients in both the theory and the experiment (including the extrapolation of amplitudes and phases of measured disturbances to the disturbance-source position), the agreement of the calculated and measured receptivity coefficients can be regarded as a satisfactory one.

It is seen that at zero frequency, the change of λ_z (in both the theory and the experiment) affects the receptivity amplitudes very weakly, while at high frequencies the efficiency of excitation of Görtler vortices depends significantly on the span-wise scale. The receptivity phases depend rather weakly on the disturbance frequency and increase slightly with it. Thus, although the traveling linear Görtler vortices grow weaker than the stationary ones [8,9], their presence can affect the laminar-turbulent transition quite substantially due to the much higher flow receptivity to localized boundary oscillations.

Note that in a flow, in which the nonparallelism of the base-flow streamlines does not affect or affect only slightly the stability characteristics, as, for example, in the case of excitation of two-dimensional TS waves in plane channel flow or Blasius boundary layer, it is possible to obtain a good approximation of downstream growth of disturbance amplitude by integrating the imaginary parts of local stream-wise wave-numbers $\alpha_i(x)$. Thus, residing completely in the framework of local stability analysis:

$$A(x) = \rho(x_0) \exp\left(\int_x^{x_0} \alpha_i(x) dx\right),$$

where $\rho(x_0)$ is, for example, the projection of the total disturbance $v(x_0)$ to the leading local mode at $x = x_0$. The projection can be found based on the adjoint leading local mode at $x = x_0$ in the similar way as the value ρ in (26) was found at $x = 1$. This provides an approach to estimate $B_{\lambda_z, f}$ in (31) as $A(1)$. This procedure works very well for the above-mentioned flows.

The corresponding growth curves with $x_0 = 4.5$ are shown in Figs. 2 and 3 by dash-dotted lines, where

$$\mathcal{E} = \mathcal{E}_N(x) = \mathcal{E}(v(x_0)) \left(\frac{|A(x)|}{|A(x_0)|}\right)^2 = \mathcal{E}(v(x_0)) \exp\left(2 \int_x^{x_0} \alpha_i(x) dx\right). \quad (32)$$

As seen, in contrast to the solutions of the initial-value problems, the slopes of dash-dotted curves far from the source do not generally follow the slopes of the total disturbances, eventually because the local analysis does not take into account the nonlocal effects captured by the parabolic equations. The other curves shown in Figs. 2 and 3 essentially either coincide or are parallel to each other at about $x = 4.4$. This is supported by the data obtained for different values of x_0 . For example, Tables 4 and 5 show the values $\mathcal{E}_N(1)$ and $\mathcal{E}(\kappa v_{\text{opt}}(1))$, respectively, for $x_0 = 4.5$ and 6.0. As seen, the values of $\mathcal{E}(\kappa v_{\text{opt}}(1))$ differ less than 5% in all cases under consideration. Thus, the optimal disturbances (and consequently the corrected modal parts of the total disturbances) are able to provide the receptivity coefficients practically independent of x_0 . On the contrary, the observed differences in values of $\mathcal{E}_N(1)$ are much larger. Thus, the receptivity coefficients derived from the local stability analysis significantly depend on x_0 . However, the values of $\mathcal{E}_N(1)$ show the same relative trends with frequency and wavelength as $\mathcal{E}(\kappa v_{\text{opt}}(1))$ and, hence, can be used in some ‘quick-and-dirty’ estimations of the receptivity coefficients.

Table 4 Values of $\mathcal{E}_N(1) \cdot 10^8$ for two different values of x_0

λ_z , mm	f , Hz	2	5	8	11	14
8	$x_0 = 4.5$	–	0.26449	0.48602	1.6737	4.5363
	$x_0 = 6.0$	–	0.17523	0.61860	2.8218	7.8110
12	$x_0 = 4.5$	0.36325	0.73936	2.1859	7.4221	21.653
	$x_0 = 6.0$	0.34259	0.74693	2.4825	10.016	38.554

Table 5 Values of $\mathcal{E}(\kappa v_{\text{opt}}(1)) \cdot 10^{11}$ for two different values of x_0

λ_z , mm	f , Hz	2	5	8	11	14
8	$x_0 = 4.5$	–	0.43274	0.84795	1.6516	2.1636
	$x_0 = 6.0$	–	0.42915	0.83726	1.6141	2.0633
12	$x_0 = 4.5$	1.4283	2.3070	4.5426	8.7517	11.924
	$x_0 = 6.0$	1.4170	2.2800	4.4573	8.4972	11.402

4 Conclusions

The linear roughness-induced boundary-layer receptivity to localized time-periodic surface nonuniformities leading to excitation of the most amplified Görtler vortices has been studied theoretically and numerically for two different span-wise wavelengths and in a range of frequencies of vibrations, including the stationary cases of zero frequency (i.e., the surface roughness) in accordance with the experiments in Refs. [36–38].

In the numerical model, the shape of the experimental surface nonuniformities is mimicked using the classical theory of thin-membrane bending to correspond as close as possible to the experimental membranes. The stream-wise position of the nonuniformities and their other relevant parameters as well as the base flow (the Blasius boundary layer) is also chosen in accordance with the experimental conditions. The computations are based on the linear parabolic equations in the primitive variables describing the evolution of Görtler vortices.

It is shown that the modal part of disturbance in the range of parameters under investigation as used in [37] provides a limited (approximate) information on the generation and propagation of the Görtler vortices. A novel receptivity model has been proposed and applied. This model represents the generated vortices as a sum of an optimal disturbance and a remainder, whose characteristics and behavior make it possible to describe both generation and propagation of the main parts of a boundary-layer disturbance over a concave wall. At the same time, the receptivity coefficients used in [37], estimated using the modal part of disturbance for stream-wise-localized disturbance sources, can be reinterpreted to preserve their practical usefulness.

The experimental and theoretical coefficients of boundary-layer receptivity to surface nonuniformities at excitation of nonstationary (in general) Görtler vortices are estimated and compared to each other for two span-wise wavelengths in a range of frequencies. A quite good agreement of the receptivity coefficients is found. It turned out that the amplitude of the receptivity coefficient grows with disturbance frequency, and at higher frequencies, it can be several times greater than that found for stationary surface roughness. Variation of the span-wise scale of surface nonuniformities affects very weakly the receptivity characteristics at the zero frequency, while at high frequencies the efficiency of excitation of Görtler vortices depends significantly on the span-wise scale and increases with it.

Comparison of the present theoretical and experimental results with previous studies of the boundary-layer instability to unsteady Görtler vortices has shown that the frequency dependencies of the efficiency of the mechanisms of linear instability and receptivity are oppositely directed, compete with each other and are able to compensate partially each other. In practical situations, this circumstance can promote the development of boundary-layer Görtler vortices in a broad range of frequencies.

It is important to note that the linear receptivity coefficients, being defined in Fourier space (for modes of frequency–wave-number spectrum), are independent, in general, of the particular shape of oscillation of the surface nonuniformities. The data obtained in the present study can be used for evaluation of initial amplitudes of stationary and nonstationary Görtler vortices excited by surface nonuniformities, as well as for verification of linear receptivity theories and for improvement of methods of prediction of transition location in flows characterized by the Görtler instability.

Acknowledgements The development and justification of numerical algorithms were supported by the Russian Science Foundation (Project No. 14–21–00025). Numerical experiments and analysis of their results were supported by the Russian Foundation for Basic Research (Grants Nos. 10–01–00109, 12–01–31211, 13–01–00270 and 13–01–00350). The authors thank anonymous referees for their insightful comments and suggestions helped us to improve significantly the paper.

References

1. Aihara, Y., Tomita, Y., Ito, A.: Generation, development and distortion of longitudinal vortices in boundary layers along concave and flat plates. In: Kozlov, V.V. (ed.) *Laminar-Turbulent Transition*, IUTAM Symposium, Novosibirsk, USSR 9–13 July 1984, pp. 447–454. Springer, Berlin (1985)
2. Bake, S., Ivanov, A.V., Fernholz, H.H., Neemann, K., Kachanov, Y.S.: Receptivity of boundary layers to three-dimensional disturbances. *Eur. J. Mech. B/Fluids* **21**, 29–48 (2002)
3. Bassom, A.P., Hall, P.: Concerning the interaction of non-stationary crossflow vortices in a three-dimensional boundary layer. *Q. J. Mech. Appl. Math.* **44**, 147–172 (1991)
4. Benjamin, T.B.: Shearing flow over a wavy boundary. *J. Fluid Mech.* **6**, 161–205 (1959)
5. Bertolotti, F.P.: Vortex generation and wave-vortex interaction over a concave plate with roughness and suction. Report 93–101, ICASE (1993)
6. Bippes, H., Görtler, H.: Dreidimensionale Störungen in der Grenzschicht an einer konkaven Wand. *Acta Mech.* **14**, 251–267 (1972)
7. Boiko, A.V., Dovgal, A.V., Grek, G.R., Kozlov, V.V.: *Physics of Transitional Shear Flows*. Springer, Berlin (2011)

8. Boiko, A.V., Ivanov, A.V., Kachanov, Y.S., Mischenko, D.A.: Quasi-steady and unsteady Goertler vortices on concave wall: experiment and theory. In: Palma, J.M.L.M., Lopes, A.S. (eds.) *Advances in Turbulence XI: Proceedings of the 11th EUROMECH European Turbulence Conference*, 25–28 June 2007 Porto, Portugal, pp. 173–175. Springer, Berlin (2007)
9. Boiko, A.V., Ivanov, A.V., Kachanov, Y.S., Mischenko, D.A.: Steady and unsteady Görtler boundary-layer instability on concave wall. *Eur. J. Mech. B/Fluids* **29**(2), 61–83 (2010)
10. Boiko, A.V., Nechepurenko, Y.M.: Numerical spectral analysis of temporal stability of laminar duct flows with constant cross-sections. *Comput. Math. Math. Phys.* **48**(10), 1699–1714 (2008)
11. Bottaro, A., Luchini, P.: Görtler vortices: are they amenable to local eigenvalue analysis? *Eur. J. Mech. B/Fluids* **18**(1), 47–65 (1999)
12. Canuto, C., Hussaini, M.Y., Quarteroni, A., Zang, T.A.: *Spectral Methods: Fundamentals in Single Domains*. Springer, Berlin (2006)
13. Choudhari, M., Duck, P.W.: Nonlinear excitation of inviscid stationary vortex instabilities in a boundary-layer flow. In: Duck, P.W., Hall, P. (eds.) *IUTAM Symposium on Nonlinear Instability and Transition in Three-Dimensional Boundary Layers: Proceedings of the IUTAM Symposium held in Manchester, 17–20 July 1995*, pp. 409–422. Springer (1996)
14. Clauser, M., Clauser, F.: The effect of curvature on the transition from laminar to turbulent boundary layer. TN 613, NACA (1937)
15. Crouch, J.D., Spalart, P.R.: A study of non-parallel and nonlinear effects on the localized receptivity of boundary layers. *J. Fluid Mech.* **290**, 29–37 (1995)
16. Denier, J.P., Hall, P., Seddougui, S.O.: On the receptivity problem for Görtler vortices: vortex motions induced by roughness. *Philos. Trans. R. Soc. Lond. A* **335**, 51–85 (1991)
17. Faris, W., Asrar, W., Omerbegovic, A.: Micropump modeling: current status and challenge. *Aust. J. Basic Appl. Sci.* **6**(1), 134–142 (2012)
18. Finnis, M.V., Brown, A.: The linear growth of görtler vortices. *Int. J. Heat Fluid Flow* **18**(04), 389–399 (1997)
19. Floryan, J.M.: On the Görtler instability of boundary layers. *J. Aerosp. Sci.* **28**, 235–271 (1991)
20. Floryan, J.M., Saric, W.S.: Stability of Görtler vortices in boundary layers. *AIAA J.* **20**(3), 316–324 (1982)
21. Gaponenko, V.R., Ivanov, A.V., Kachanov, Y.S.: Experimental study of 3D boundary-layer receptivity to surface vibrations. In: Duck, P.W., Hall, P. (eds.) *IUTAM Symposium on Nonlinear Instability and Transition in Three-Dimensional Boundary Layers: Proceedings of the IUTAM Symposium held in Manchester, 17–20 July 1995*, pp. 389–398. Kluwer, Dordrecht (1996)
22. Gaponenko, V.R., Ivanov, A.V., Kachanov, Y.S., Crouch, J.D.: Swept-wing boundary-layer receptivity to surface nonuniformities. *J. Fluid Mech.* **461**, 93–126 (2002)
23. Gaurav, Shankar, V.: Stability of pressure-driven flow in a deformable neo-hookean channel. *J. Fluid Mech.* **659**, 318–350 (2010)
24. Görtler, H.: Inistabilität laminaren Grenzsichten an konkaven Wänden gegenüber gewissen dreidimensionalen Störungen. *Z. Angew. Math. Mech.* **21**, 250–252 (1941)
25. Gregory, N., Walker, W.S.: The effect on transition of isolated surface excrescences in the boundary-layer. R&M 2779, ARC (1956)
26. Hairer, E., Nørsett, S.P., Wanner, G.: *Solving Ordinary Differential Equations I: Nonstiff Problems*, 2nd edn. Springer, Berlin (2008)
27. Hall, P.: Taylor-Görtler vortices in fully developed or boundary-layer flows: linear theory. *J. Fluid Mech.* **124**, 475–494 (1982)
28. Hall, P.: The linear development of Görtler vortices in growing boundary layers. *J. Fluid Mech.* **130**, 41–58 (1983)
29. Hall, P.: The nonlinear development of Görtler vortices in growing boundary layers. *J. Fluid Mech.* **193**, 243–266 (1988)
30. Hall, P.: Görtler vortices in growing boundary layers: the leading edge receptivity problem, linear growth and the nonlinear breakdown stage. *Mathematika* **37**, 151–189 (1990)
31. Hämmerlin, G.: Über das Eigenwertproblem der dreidimensionalen Instabilität laminarer Grenzsichten an konkaven Wänden. *J. Ration. Mech. Anal.* **4**(2), 279–321 (1955)
32. Hämmerlin, G.: Zur Theorie der dreidimensionalen Instabilität laminarer Grenzsichten. *Z. Angew. Math. Phys.* **7**, 156–164 (1956)
33. Herron, I.H., Clark, A.D.: Instabilities in the Görtler model for wall bounded flows. *Appl. Math. Lett.* **13**, 105–110 (2000)
34. Höpfner, J., Bottaro, A., Favier, J.: Mechanisms of non-modal energy amplification in channel flow between compliant walls. *J. Fluid Mech.* **642**, 489–507 (2010)
35. Ito, A.: Visualization of boundary layer transition along a concave wall. In: *Proceedings of the 4th International Symposium on Flow Visualization (Paris)*, pp. 339–344. Hemisphere, Washington (1987)
36. Ivanov, A.V., Kachanov, Y.S., Mischenko, D.A.: Excitation of unsteady Görtler vortices by surface non-uniformities. In: *Euromech Fluid Mechanics Conference-8 (EFMC-8)*, 13–16 September. Abstracts, pp. S4–12. Bad-Reichenhall, Germany (2010)
37. Ivanov, A.V., Kachanov, Y.S., Mischenko, D.A.: Boundary-layer receptivity to surface non-uniformities leading to generation of Görtler vortices. *J. Phys. Conf. Ser.* **318**, 1–10 (2011)
38. Ivanov, A.V., Kachanov, Y.S., Mischenko, D.A.: Generation of nonstationary Görtler vortices by localized surface nonuniformities. Receptivity coefficients. *Thermophys. Aeromech.* **19**(4), 523–539 (2012)
39. Ivanov, A.V., Kachanov, Y.S., Obolentseva, T.G.: Experimental study of the blasius boundary layer receptivity to localized surface vibrations. *Thermophys. Aeromech.* **6**(2), 179–192 (1999)
40. Ivanov, A.V., Kachanov, Y.S., Obolentseva, T.G., Michalke, A.: Receptivity of the Blasius boundary layer to surface vibrations. Comparison of theory and experiment. In: Kharitonov A.M. (ed.) *Proceedings of Ninth International Conference on Methods of Aerophysical Research*, vol. 1, pp. 93–98. RAS, Sib. Branch Inst. Theoret. Appl. Mech., Novosibirsk (1998)
41. Kachanov, Y.S.: Three-dimensional receptivity of boundary layers. *Eur. J. Mech. B/Fluids* **19**(5), 723–744 (2000)
42. Kierzenka, J., Shampine, L.F.: A BVP solver based on residual control and the Matlab PSE. *ACM TOMS* **27**(3), 299–316 (2001)

43. Liepmann, H.W.: Investigations on laminar boundary layer stability and transition on curved boundaries. Wartime Report W-107, NACA (1943)
44. Luchini, P.: Linearized no-slip boundary conditions at a rough surface. *J. Fluid Mech.* **737**, 349–367 (2013)
45. Luchini, P., Bottaro, A.: Görtler vortices: a backward in time approach to the receptivity problem. *J. Fluid Mech.* **363**, 1–23 (1998)
46. Murphy, J.S.: Extensions of the Falkner-Skan similar solutions to flows with surface curvature. *AIAA J.* **3**(11), 2043–2049 (1965)
47. Nechepurenko, Y.M.: On the dimension reduction of linear differential-algebraic control systems. *Doklady Math.* **86**(1), 457–459 (2012)
48. Saric, W.S.: Görtler vortices. *Annu. Rev. Fluid Mech.* **26**, 379–409 (1994)
49. Saric, W.S., Reed, H.L., Kerschen, E.J.: Boundary-layer receptivity to freestream disturbances. *Annu. Rev. Fluid Mech.* **34**, 291–319 (2002)
50. Saric, W.S., Reed, H.L., White, E.B.: Stability and transition of three-dimensional boundary layers. *Annu. Rev. Fluid Mech.* **35**, 413–440 (2003)
51. Schlichting, H., Gersten, K.: *Boundary Layer Theory*, 8th edn. Springer, Berlin (2000)
52. Schmid, P.J., Henningson, D.S.: *Stability and Transition in Shear Flows*. Springer, Berlin (2001)
53. Schultz, M.P., Volino, R.J.: Effects of concave curvature on boundary layer transition under high free-stream turbulence conditions. *ASME J. Fluids Eng.* **125**, 18–27 (2003)
54. Shampine, L.F., Gladwell, I., Thompson, S.: *Solving ODEs with MATLAB*. Cambridge University Press, Cambridge (2003)
55. Smith, A.M.O.: On the growth of Taylor–Görtler vortices along highly concave walls. *Q. Appl. Math.* **13**, 223 (1955)
56. Spall, R.E., Malik, M.R.: Goertler vortices in supersonic boundary layers. Paper 88-3678, AIAA (1988)
57. Tani, I.: Production of longitudinal vortices in the boundary-layer along a curved wall. *J. Geophys. Res.* **67**, 3075–3080 (1962)
58. Tannehill, J.C., Anderson, D.A., Pletcher, R.H.: *Computational Fluid Mechanics and Heat Transfer*, 3rd edn. Series in Computational and Physical Processes in Mechanics and Thermal Sciences. CRC Press, Boca Raton (2012)
59. Taylor, G.I.: Stability of a viscous liquid contained between two rotating cylinders. *Proc. R. Soc. Lond. A* **223**, 289–343 (1923)
60. Tempelmann, D., Schrader, L.U., Hanifi, A., Brandt, L., Henningson, D.S.: Swept wing boundary-layer receptivity to localized surface roughness. *J. Fluid Mech.* **711**, 516–544 (2012)
61. Timoshenko, S.P., Woinowsky-Krieger, S.: *Theory of Plates and Shells*, Engineering Societies Monographs, 2nd edn. McGraw-Hill, New York (1959)
62. Tomita, Y., Funatsu, K., Tsuzuki, S., Miyazaki, K.: Neutral stability of laminar boundary layers along the concave wall. *Bull. J. Jpn. Soc. Mech. Eng.* **28**, 2288–2293 (1985)
63. Tumin, A., Reshotko, E.: Spatial theory of optimal disturbances in boundary layers. *Phys. Fluids* **13**(7), 2097–2104 (2001)
64. Weideman, J.A.C., Reddy, S.C.: A MATLAB differentiation matrix suite. *ACM Trans. Math. Softw.* **26**(4), 465–519 (2000)
65. Wu, X.: Receptivity of boundary layers with distributed roughness to vortical and acoustic disturbances: a second-order asymptotic theory and comparison with experiments. *J. Fluid Mech.* **431**, 91–133 (2001)
66. Wu, X., Zhao, D., Luo, J.: Excitation of steady and unsteady Görtler vortices by free-stream vortical disturbances. *J. Fluid Mech.* **682**, 66–100 (2011)
67. Yeo, K.S.: The stability of boundary-layer flow over single- and multi-layer viscoelastic walls. *J. Fluid Mech.* **196**, 359–408 (1988)